metals

MDPI

Article

Comparative Effect of Mo and Cr on Microstructure and Mechanical Properties in NbV-Microalloyed Bainitic Steels

Andrii Kostryzhev [1,*], Navjeet Singh [1], Liang Chen [2], Chris Killmore [3] and Elena Pereloma [2,4]

[1] Australian Steel Research Hub, University of Wollongong, Wollongong, NSW 2500, Australia; ns106@uowmail.edu.au
[2] School of Mechanical, Materials, Mechatronic and Biomedical Engineering, University of Wollongong, Wollongong, NSW 2500, Australia; lchen@uow.edu.au (L.C.); elenap@uow.edu.au (E.P.)
[3] BlueScope Steel Limited, Five Islands Road, Port Kembla, NSW 2505, Australia; chris.killmore@bluescopesteel.com
[4] UOW Electron Microscopy Centre, University of Wollongong, Wollongong, NSW 2519, Australia
* Correspondence: andrii@uow.edu.au; Tel.: +61-02-4221-3034

Received: 4 January 2018; Accepted: 13 February 2018; Published: 16 February 2018

Abstract: Steel product markets require the rolled stock with further increasing mechanical properties and simultaneously decreasing price. The steel cost can be reduced via decreasing the microalloying elements contents, although this decrease may undermine the mechanical properties. Multi-element microalloying with minor additions is the route to optimise steel composition and keep the properties high. However, this requires deep understanding of mutual effects of elements on each other's performance with respect to the development of microstructure and mechanical properties. This knowledge is insufficient at the moment. In the present work we investigate the microstructure and mechanical properties of bainitic steels microalloyed with Cr, Mo, Nb and V. Comparison of 0.2 wt. % Mo and Cr additions has shown a more pronounced effect of Mo on precipitation than on phase balance. Superior strength of the MoNbV-steel originated from the strong solid solution strengthening effect. Superior ductility of the CrNbV-steel corresponded to the more pronounced precipitation in this steel. Nature of these mechanisms is discussed.

Keywords: steel; thermomechanical processing; microstructure characterisation; mechanical properties; molybdenum

1. Introduction

In high strength low alloyed steels Mo is well known to provide phase balance strengthening, via facilitating the bainite transformation [1–5], and solid solution strengthening [6–9]. It can decrease the rate of dynamic recrystallization of austenite [10–12], which may lead to grain refinement. Sometimes Mo can contribute to precipitation strengthening through formation of Mo-rich carbides [13–16]. Although its main effect on precipitation is via the increase in solubility of Ti [17,18] and Nb [10] in austenite, resulting in decreased sizes and increased number densities of Ti- and Nb-rich particles [19–23], which are essential for the precipitation strengthening from Ti- and Nb-rich particles.

Similar to Mo, Cr facilitates the bainite transformation [24–26], may precipitate in complex Cr-rich carbides [27–29], and increases solubility of Ti [30,31] and Nb [30,32,33]. In particular, Cr was observed delaying Fe_3C precipitation in low carbon steel [34]. However, the solid solution strengthening effect of Cr is ~6 times weaker than this of Mo [35], and, therefore, Cr is less affective in retarding recrystallization [36,37].

Amongst the published data, effects of Mo and Cr in multi-microalloyed steels, in particular containing V, are rarely reported. In 0.042C-0.3Mo-1.0Cr-0.08V steel coiled in the temperature range

of 180–530 °C, Hutchinson et al. [38] observed bainitic microstructures with average ferrite grain size of 3 μm. Increased to 640–770 MPa proof stress was suggested to originate mainly from high dislocation density in bainite and, in particular, dislocation pinning by V(C,N) precipitates. In another work, Kong et al. [39] investigated mechanical properties of 0.064C-0.22Mo-0.21Cr-0.031Nb-0.031V steel thermomechanically processed in a temperature range of 1150–800 °C and cooled at the rate of 20–30 °C/s to 430–550 °C finish cooling temperature. The yield stress in the range of 530–710 MPa was attributed to the narrow width of bainitic ferrite lath (about 0.52 μm), although precipitation of TiNbV-rich particles was also observed. Abbasi and Rainforth [40] studied the microstructure and mechanical properties in MoNbV microalloyed ferritic steel. Simultaneous additions of 0.08 wt. % Mo and 0.04 wt. % Nb to 0.12C-0.16V ferritic steel resulted in precipitation of MoNbVC and decreased size of VC particles, which was explained by the improved temperature stability and reduced coarsening rate of multi-element precipitates. Increased steel hardness with Nb and Mo microalloying was related to finer ferrite grain size and higher number density of VC particles in the NbMoV-microalloyed steel. In this work we advance the knowledge of multi-microalloyed steels in the following aspects: (i) compare the effects of minor Mo and Cr additions on phase transformation and particle precipitation in low carbon NbV-microalloyed bainitic steels; (ii) analyse the microstructure-property relationship in the newly developed steels with 700–850 MPa of yield stress; and (iii) investigate the effect of high temperature strain (in the recrystallization temperature region) on room temperature microstructure and mechanical properties. The effect of high temperature (>1000 °C) strain is important to study because increased strain values may enhance recrystallization of austenite (refine grain size) and accelerate precipitation of MoNbV-rich particles [10,23,28,41] (reduce Mo solid solute concentrations). Consequently, the grain size, precipitate number density and solute atom concentrations will affect the ambient temperature mechanical properties.

2. Materials and Methods

Two steels containing 0.08C, 1.5Mn, 0.3Si, 0.2Ni, 0.03Al, 0.003S, 0.015P, 0.01N, 0.06Nb, 0.12V and either 0.3Cr-0.2Mo or 0.5Cr-0Mo (wt. %), denoted below as MoNbV-steel and CrNbV-steel respectively, were melted in a 60 kg induction furnace and cast as 75 × 100 × 150 mm^3 blocks by Hycast Metals Pty, Sydney, Australia. The blocks were homogenised at 1250 °C for 30 h, to equalise chemical composition, then forged in the temperature range of 1250–900 °C along the 100 mm side to 28 mm plate thickness, to assure 3.5 times reduction of the as-cast microstructure. The forged plates were cut into standard 20 × 15 × 10 mm^3 Gleeble samples. Thermomechanical processing in Gleeble (manufactured by Dynamic Systems Inc., Poestenkill, NY, USA) was conducted using two schedules:

- Austenitising at 1250 °C for 180 s, followed by cooling to 1175 °C at a cooling rate of 1 °C·s^{-1};
- First deformation at 1175 °C to 0.3 (low strain schedule) or 0.35 (high strain schedule) strain at 5 s^{-1} strain rate, followed by cooling to 1100 °C at a cooling rate of 2 °C·s^{-1};
- Second deformation at 1100 °C to 0.35 (low strain schedule) or 0.50 (high strain schedule) strain at 5 s^{-1} strain rate, followed by cooling to 1000 °C at a cooling rate of 25 °C·s^{-1};
- Third deformation at 1000 °C to 0.25 strain at 5 s^{-1} strain rate, followed by cooling to 900 °C at a cooling rate of 30 °C·s^{-1};
- Fourth deformation at 900 °C to 0.25 strain at 5 s^{-1} strain rate, followed by holding at this temperature for 10 s and cooling to 500 °C at a cooling rate of 30 °C·s^{-1} to assure bainite transformation;
- Holding at 500 °C for 900 s to simulate coiling, followed by air cooling to room temperature.

The processing schedule parameters (deformation temperature range, total strain and strain per pass, strain rate, and cooling rate between passes) have been defined to model the industrial rolling process within reasonable limits of the Gleeble simulator.

Microstructure characterisation for the four studied conditions was carried out using optical, scanning (SEM) and transmission (TEM) electron microscopy. For optical and SEM microscopy,

the Gleeble samples were cut parallel to the normal direction (ND)–rolling direction (RD) plane, where ND is the compression direction and RD represents the rolling direction in Gleeble simulation. For TEM and tensile properties testing the samples were cut parallel to the normal direction (ND)–transverse direction (RD) plane. Optical and SEM sample preparation included polishing with SiC papers and diamond suspensions followed by etching with 5% Nital. Foils for TEM were prepared by hand polishing with a number of SiC papers, pre-thinning on a dimple grinder, and ion milling on a Gatan PIPS machine (manufactured by Gatan, Pleasanton, CA, USA). Optical microscopy was conducted on a Leica DM6000M microscope (manufactured by Leica Microsystems, Wetzlar, Germany) equipped with Leica Application Suite (LAS) 4.0.0 image processing software (developed by Leica Microsystems). Scanning electron microscopy was carried out using a JEOL 7001F FEG scanning electron microscope (manufactured by JEOL, Tokyo, Japan) operating at 15 kV for imaging and 7 kV for energy dispersive X-ray spectroscopy (EDS) of precipitates. For the determination of size of bainitic ferrite (the shortest distance between the martensitic grains) more than 400 randomly located areas were manually measured in SEM images for each of four studied conditions. In the SEM visible size range precipitation was scarce. Thus, only a limited number of 50 particles was analysed for the determination of precipitate sizes, number density and area fraction values for each of four studied conditions. The EDS semi-quantitative point analysis was carried out for 20 particles for each studied condition using an AZtec 2.0 Oxford SEM EDS system (manufactured by Oxford Instruments, Abingdon, UK). Transmission electron microscopy was conducted on a JEOL JEM2010 TEM microscope (manufactured by JEOL, Tokyo, Japan). For the analysis of <15 nm particle parameters, 200–500 precipitates were imaged for each of four studied conditions. The precipitates type was analyzed using selected area diffraction. The foil thickness was measured to be ~80 nm; a convergent beam diffraction technique was applied for this measurement [42]. Imaging of dislocation structure was performed for the beam direction being close to [011] grain zone axis. Tensile testing for the four studied conditions was carried out on a Kammrath and Weiss GmbH tensile stage. Testing was performed using 3 mm wide, 1 mm thick and 7 mm gauge length flat specimens. The constant crosshead speed of 7 $\mu m \cdot s^{-1}$ was applied and resulted in 1×10^{-3} s^{-1} strain rate. Two specimens were tested per condition.

3. Results

3.1. Grain Structure and Phase Balance

Optical, SEM and TEM microscopy showed in both steels a microstructure of mixed granular bainite and bainitic ferrite (Figure 1). Blocky or elongated martensite was present as the second phase. In both steels, the martensite crystals comprise a number of sub-grains with low angle (~10°) boundaries between them in accordance with possible intervariant misorientation of 10.53° [43] for Kurdjumov–Sachs relationship between the parent austenite (face centred cubic (fcc) crystal structure) and product martensite (body centred cubic (bcc) crystal structure, observe the rotation of diffraction patterns in neighbouring sub-grains in Figures 2 and 3). The diffraction analysis (points A, B and C in Figure 2b, and points A and B in Figure 3b) confirmed the bcc type of crystal structure of martensite. Retained austenite was not observed. The average size of bainitic ferrite (the shortest distance between bainitic ferrite-martensite boundaries across the bainitic ferrite area) was measured to be below 1 μm (Table 1). The variation in the average sizes and shape of size distributions (Figure 4b) of bainitic ferrite with steel composition and processing schedule was insignificant and could result from the measurement error. However, a noticeable variation in the size of martensite grains was observed (Figure 4c,d). Thus, for low strain processing, the maximum size of blocky grains was 16% smaller and the maximum length of elongated grains was 40% shorter in the CrNbV-steel. For high strain processing an opposite trend was observed: the average and maximum sizes of blocky grains were 64% and 3.7 times, respectively, larger in the CrNbV-steel; and average and maximum length of elongated

grains were 20% and 30%, respectively, larger in the CrNbV-steel. In addition for high strain processing, the total fraction of martensite was 1.5 times higher in the CrNbV-steel.

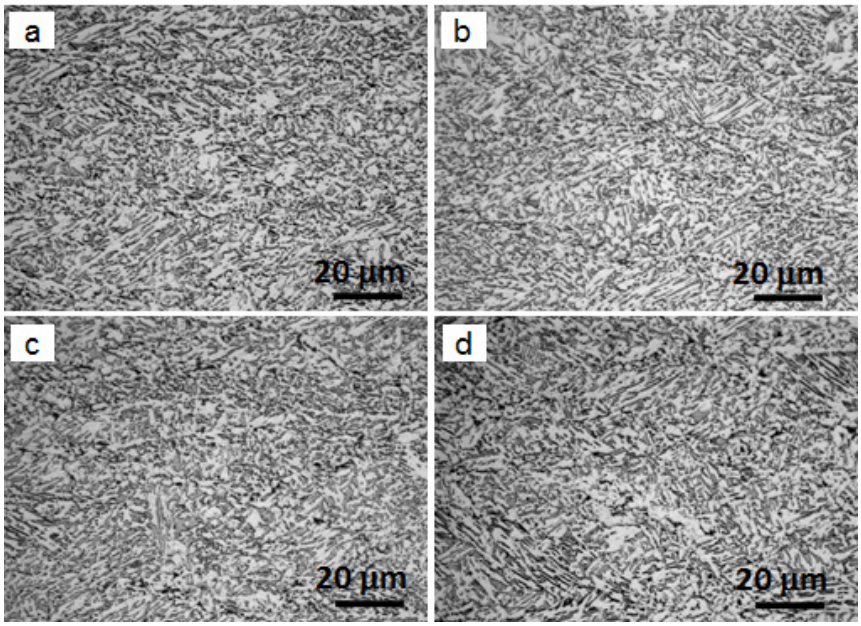

Figure 1. Optical images of microstructures in (**a**,**b**) MoNbV-steel and (**c**,**d**) CrNbV-steel after (**a**,**c**) low and (**b**,**d**) high strain processing.

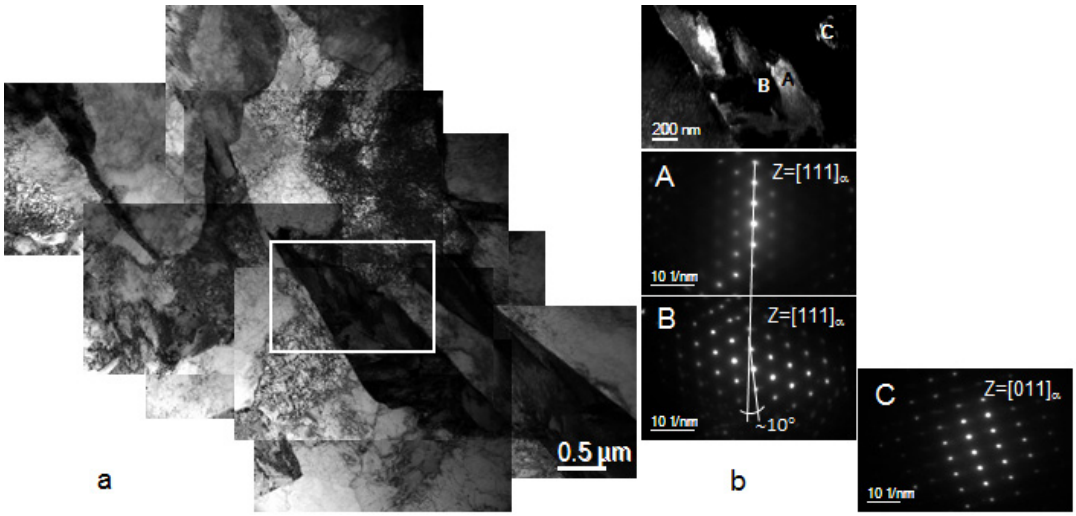

Figure 2. TEM (**a**) bright field image of microstructure and (**b**) dark field image of martensite in MoNbV-steel after low strain processing; (**b**) is from the white frame in (**a**); A, B and C diffraction patterns were taken from the corresponding points in the dark field image.

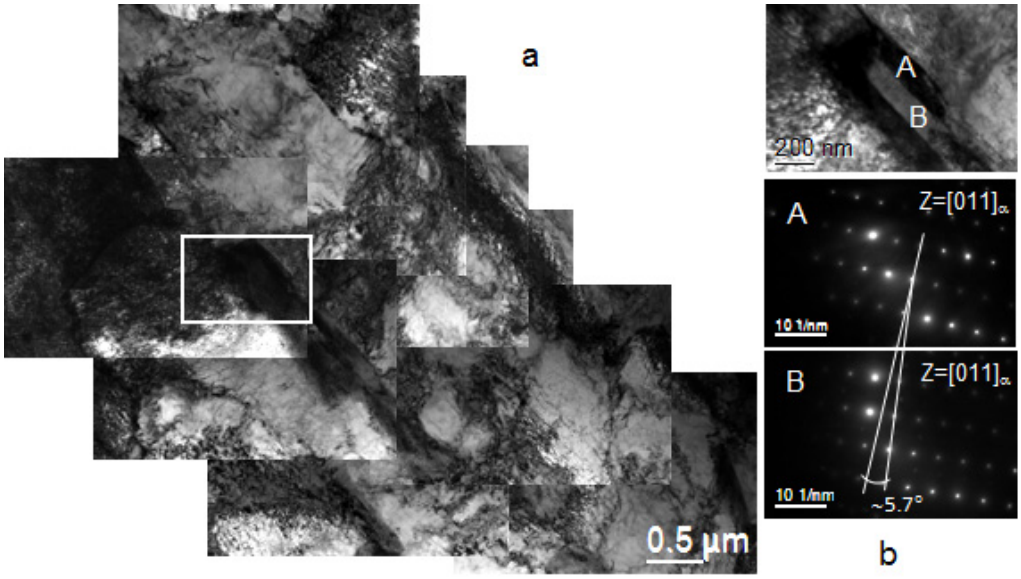

Figure 3. TEM (**a**) bright field image of microstructure and (**b**) dark field image of martensite in CrNbV-steel after low strain processing; (**b**) is from the white frame in (**a**); A and B diffraction patterns were taken from the corresponding points in the dark field image.

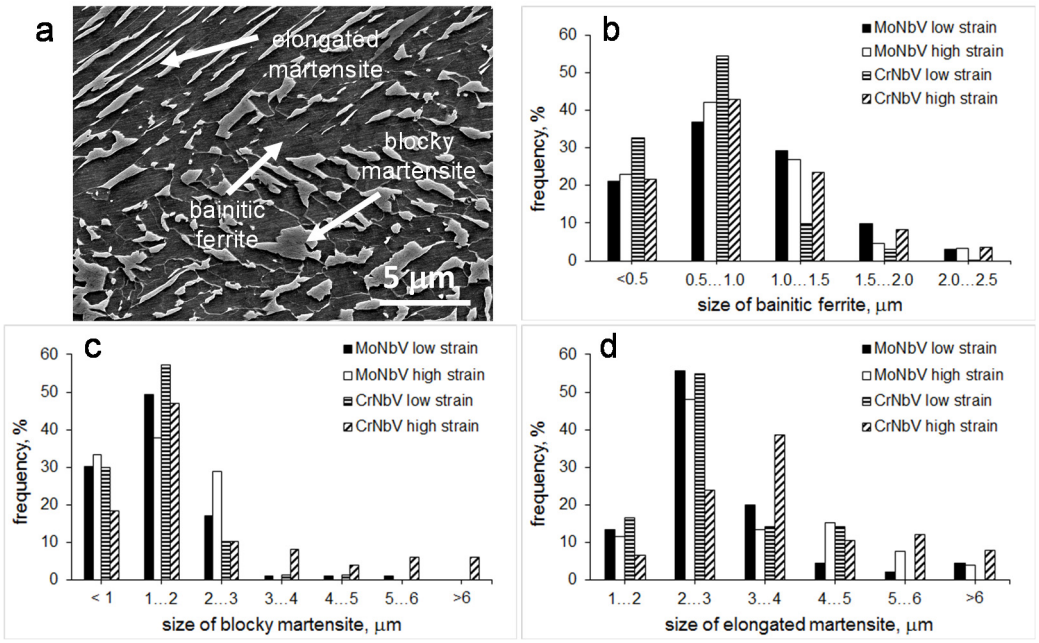

Figure 4. (**a**) A representative SEM image of microstructure in CrNbV-steel and size frequency distributions of (**b**) bainitic ferrite; (**c**) blocky martensite and (**d**) elongated martensite for four studied conditions.

Table 1. Microstructural parameters and mechanical properties of the studied steels.

Parameters		MoNbV Steel		CrNbV Steel	
		Low Strain	**High Strain**	**Low Strain**	**High Strain**
size of bainitic ferrite areas [#], μm		0.95 ± 0.45	0.84 ± 0.42	0.72 ± 0.33	0.91 ± 0.45
martensite	fraction, %	20	11	20	17
	average size of blocky grains, μm	1.4 ± 0.7	1.4 ± 0.6	1.2 ± 0.7	2.3 ± 2.0
	maximum size of blocky grains, μm	5.0	2.8	4.2	10.4
	average length of elongated grains, μm	2.8 ± 1.2	3.0 ± 1.3	2.7 ± 0.9	3.7 ± 1.8
	maximum length of elongated grains, μm	8.3	8.0	4.8	10.4
>20 nm particles (SEM)	average size, nm	42 ± 15	21 ± 4	27 ± 12	26 ± 13
	number density, μm^{-2}	0.27	0.91	0.95	1.67
	area fraction	0.0003	0.0003	0.0006	0.0011
	chemistry	75% with MoNbV 25% with Mo	36% with MoNbV 64% with Mo	59% with NbV 41% with Nb	58% with NbV 42% with Nb
<20 nm particles (TEM)	average size, nm	2.4 ± 0.5	3.2 ± 1.0	2.7 ± 0.7	2.8 ± 1.0
	number density, μm^{-3}	15,667	9875	25,595	16,744
	volume fraction	0.0001	0.0002	0.0003	0.0003
	chemistry	Cementite, Fe_3C			
dislocation density, $\times 10^{15}$ m^{-2}		0.93 ± 0.15	0.43 ± 0.10	0.85 ± 0.11	0.41 ± 0.10
matrix unite cell size, nm		0.310	0.312	0.308	0.306
YS, MPa		850 ± 30	775 ± 35	765 ± 30	700 ± 20
UTS, MPa		1200 ± 45	1090 ± 40	1000 ± 25	975 ± 20
Elongation, %		14 ± 2	13.5 ± 2	16 ± 3	19.5 ± 2

[#] The shortest distance between the martensitic grains. YS: yield stress; UTS: ultimate tensile strength.

3.2. Particle Precipitation

The SEM analysis revealed 20–70 nm precipitates in the bainitic ferrite in all four studied conditions (Figure 5). However, the particle chemistry and number density varied with condition. In the MoNbV-steel, the particles were mainly of two types: NbV-containing with/without Mo and Mo-containing without Nb or V. In the CrNbV-steel, the particles were also of two types: NbV-containing and Nb-containing (Figure 6). Detailed characterisation of the particle compositions was outside of this paper scope; however, on the basis of previously published data we believe that NbV-containing particles were MX type NbV(CN) [44–46], MoNbV-containing ones were MoNbVC [13,47], and Mo-containing ones could be complex FeMoC [48]. The average particle number density and area fraction were lower in the MoNbV-steel, compared to the CrNbV-steel, for both processing conditions (Table 1). In the MoNbV-steel, with an increase in deformation strain the average >20 nm particle size decreased (from 42 ± 15 to 21 ± 4 nm), number density increased (from 0.27 to 0.91 μm^{-2}), and the relative amount of Mo-containing particles to the total amount analysed also increased (from 25% to 64%). In the CrNbV-steel, the average >20 nm particle size and relative amount of Nb-containing particles did not show a significant variation with strain, although both the number density and area fraction increased (from 0.95 to 1.67 μm^{-2} and from 0.0006 to 0.0011, respectively) with strain.

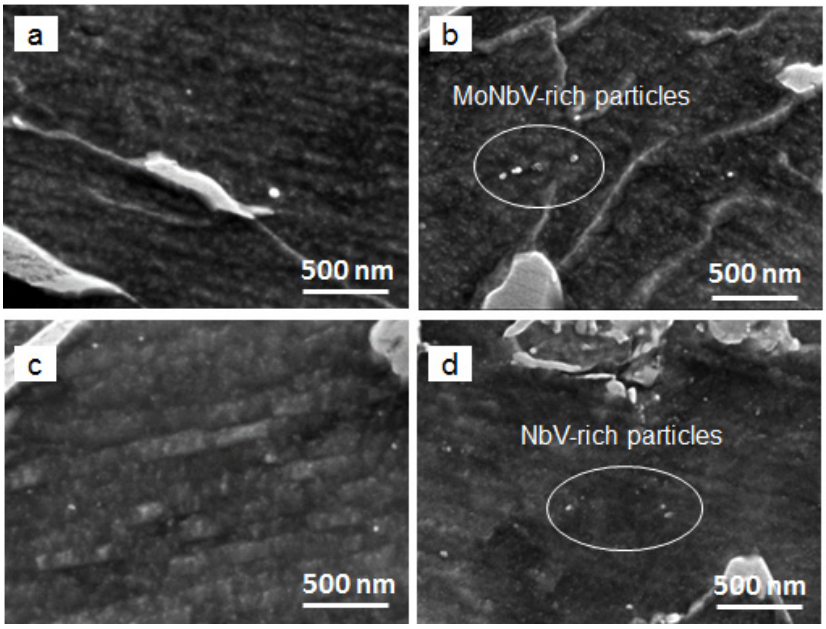

Figure 5. SEM images of precipitates in (**a**,**b**) MoNbV-steel and (**c**,**d**) CrNbV-steel after (**a**,**c**) low and (**b**,**d**) high strain processing.

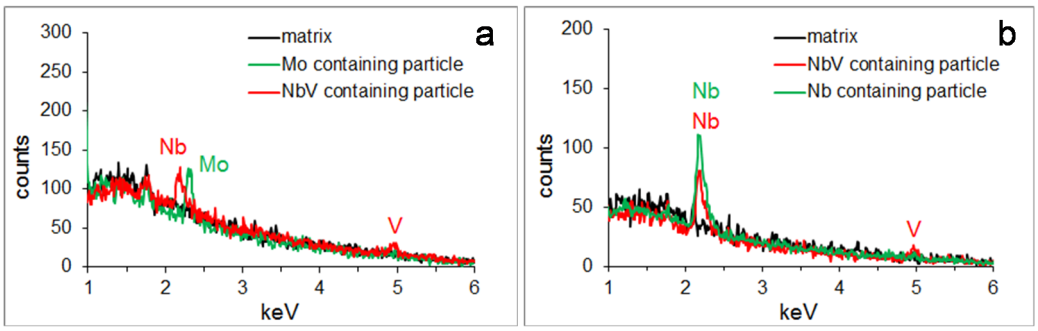

Figure 6. Energy dispersive X-ray spectroscopy (EDS) spectra of (**a**) Mo and NbV containing particles in the MoNbV-steel and (**b**) Nb and NbV containing particles in the CrNbV-steel.

The TEM investigation showed presence of 2–8 nm precipitates in the bainitic ferrite in all four conditions (Figure 7). As the particles were too small for EDS, their nature was analysed using the selected area diffraction technique. Numerous calculations (omitted here) suggested absence of Mo-, Cr-, Nb- or V-rich carbides or nitrides in the TEM studied particle size range in both steels. Thus, the particles were identified as Fe_3C exhibiting Bagaryatskii [49] orientation relationship to the bcc (bainitic ferrite) matrix: $[011]_{matrix} \parallel [001]_{Fe3C}$ and $[001]_{matrix} \parallel [321]_{Fe3C}$ (Figure 8). Measurements of d-spacing have shown $d_{0\bar{1}2}$ = 0.306 nm, $d_{1\bar{1}\bar{1}}$ = 0.317 nm and d_{200} = 0.358 nm, which was slightly larger than the theoretical values $d_{0\bar{1}2}$ = 0.281 nm, $d_{1\bar{1}\bar{1}}$ = 0.302 nm and d_{200} = 0.337 nm calculated using the Fe_3C lattice parameters a = 0.674 nm, b = 0.509 nm and c = 0.453 nm [50]. The unit cell size of bcc (bainitic ferrite) matrix, measured using the TEM diffraction patterns, was also expanded to 0.306–0.312 nm (Table 1) from the theoretical value of 0.286 nm. The Fe_3C expansion by 5–9% corresponds to this of matrix by 7–9%. It is important to note, that the matrix expansion was larger in the MoNbV-steel than that in the CrNbV-steel. The matrix expansion could result from an increased concentration of solid solute atoms [51]. The average Fe_3C size did not vary significantly with steel composition and processing (was within the measurement error). However, the average Fe_3C number density and area fraction were lower in the MoNbV-steel, compared to the CrNbV-steel,

for both processing conditions (Table 1). With an increase in deformation strain the average 2–8 nm particle number density decreased from 15,667 to 9875 μm^{-3} in the MoNbV-steel and from 25,595 to 16,744 μm^{-3} in the CrNbV-steel. Within the 2–8 nm size range an opposite trend was observed for 2–3 nm and 3–8 nm particles: amount of 2–3 nm ones decreased with strain and this of 3–8 nm ones increased with strain (compared Figure 9a,b). An opposite trend with strain was also observed for the 2–8 nm particles (studied by TEM) compared to the >20 nm ones (studied by SEM): with an increase in strain the number density of >20 nm particles increased and this of 2–8 nm ones decreased.

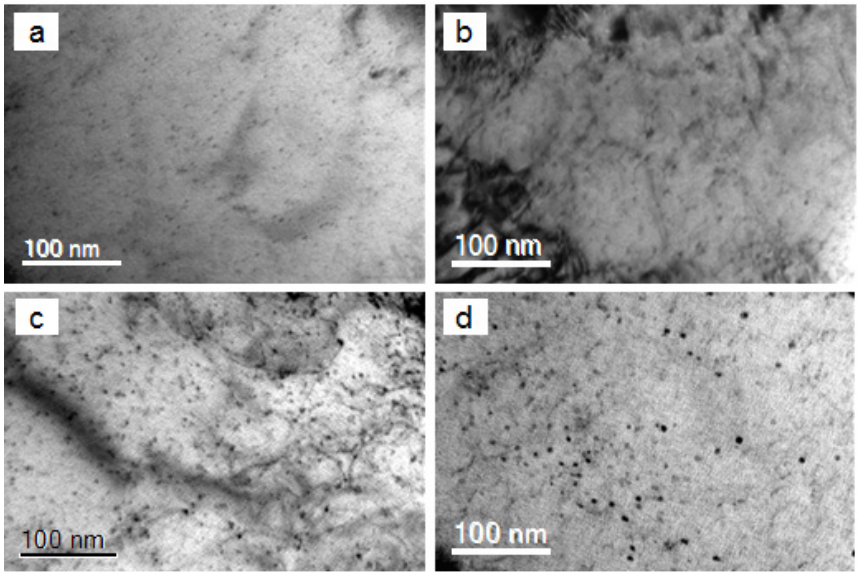

Figure 7. TEM bright field images of precipitates in (**a**,**b**) MoNbV-steel and (**c**,**d**) CrNbV-steel after (**a**,**c**) low and (**b**,**d**) high strain processing.

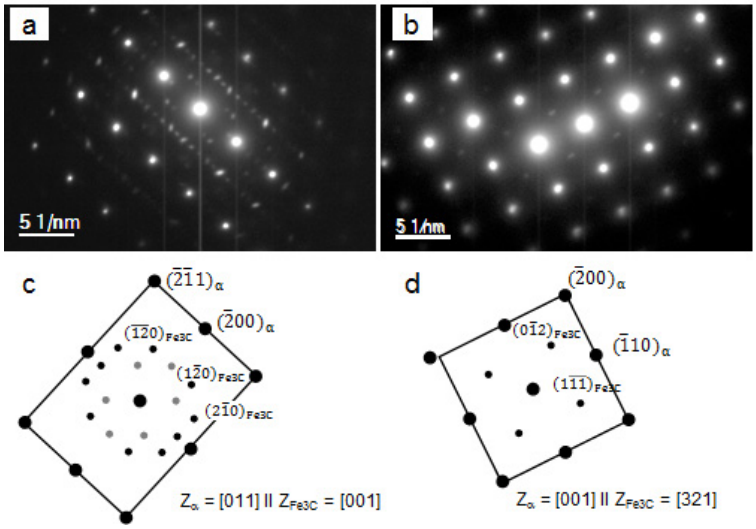

Figure 8. Selected area diffraction patterns of Fe_3C precipitates in (**a**) MoNbV-steel and (**b**) CrNbV-steel; (**c**) determination of the matrix-particle orientation relationship for image (**a**) and (**d**) this for image (**b**).

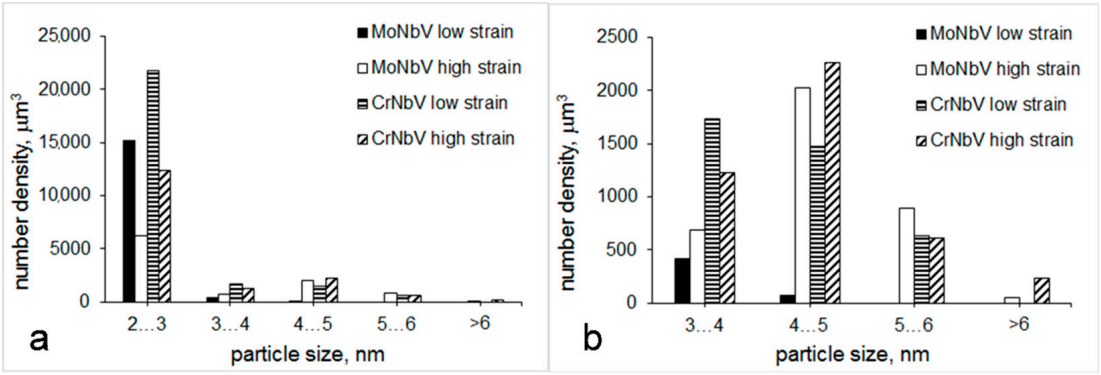

Figure 9. Number density distributions of precipitates studied by TEM for (**a**) >2 nm size range and (**b**) >3 nm size range.

3.3. Dislocation Structure

Typical dislocation structure in the middle of bainitic ferrite areas is shown in Figure 10 and some selected features are presented in Figure 11. In both steels, the average dislocation density in bainitic ferrite was at the level of $(0.9 \pm 0.15) \times 10^{15}$ m^{-2} after low strain processing and $(0.4 \pm 0.10) \times 10^{15}$ m^{-2} after high strain processing (Table 1). These values correspond to the reported in the literature for bainitic microstructures [52–54]. In the MoNbV-steel very high density dislocation walls surrounding a low density interior (arrangements resembling cells) where occasionally observed (Figure 11a), although they were not present in the CrNbV-steel. Bainitic ferrite areas closer to the martensite grains exhibited a higher local dislocation density than the overall average (Figure 11b). In both steels the dislocation arrays (Figure 11c,e), disintegrated walls (Figure 11d) and tangles (Figure 11f) were also observed, mainly after high strain processing.

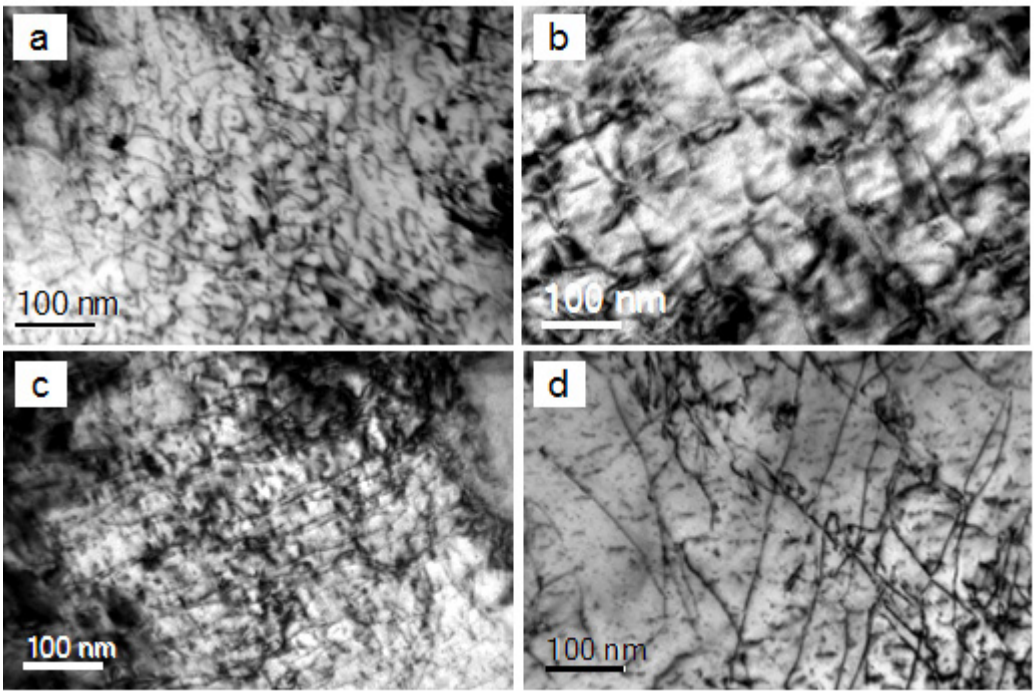

Figure 10. Representative TEM images of dislocation structure in (**a**,**b**) MoNbV-steel and (**c**,**d**) CrNbV-steel after (**a**,**c**) low and (**b**,**d**) high strain processing.

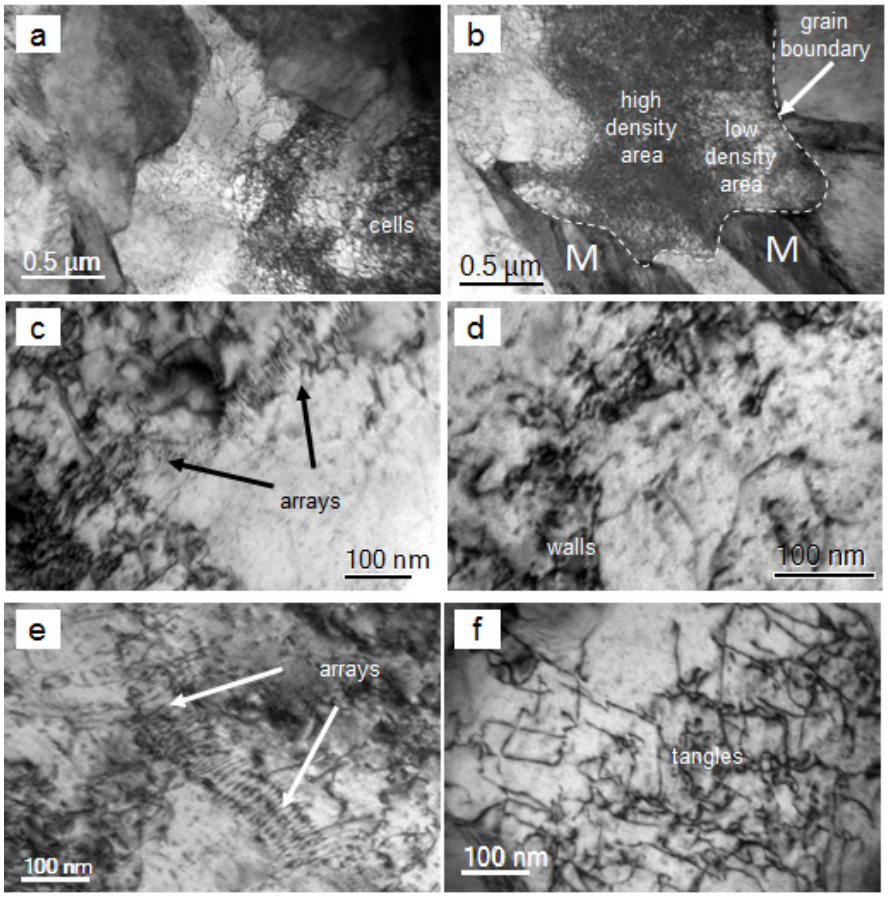

Figure 11. Selected TEM images of dislocation structure in MoNbV-steel after (**a**,**b**) low and (**c**,**d**) high strain processing; and in CrNbV-steel after (**e**) low and (**f**) high strain processing.

3.4. Mechanical Properties

The MoNbV-steel showed higher strength, and slightly lower elongation, than the CrNbV-steel (Table 1, Figure 12). The variations in yield stress (YS) and ultimate tensile strength (UTS) with steel composition were higher for the low strain schedule: 85 MPa in YS and 200 MPa in UTS for the low strain and 75 MPa in YS and 115 MPa in UTS for the high strain schedule. It is worth to note an opposite trend in the elongation variation with strain: in the MoNbV-steel elongation slightly decreased with strain, and in the CrNbV-steel it increased with strain.

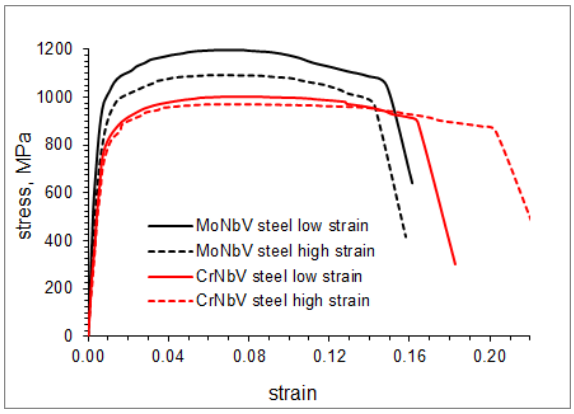

Figure 12. Engineering stress-strain curves for four studied conditions.

4. Discussion

According to various empirical equations [55–57]:

$$B_s = 830 - 270C - 90Mn - 37Ni - 70Cr - 83Mo,$$

$$B_s = 732 - 202C + 216Si - 85Mn - 37Ni - 47Cr - 39Mo,$$

$$B_s = 745 - 110C - 59Mn - 39Ni - 68Cr - 106Mo + 17MnNi + 6Cr^2 + 29Mo^2,$$

the bainite transformation start temperature, B_s, was similar in both steels: 605–628 °C in the MoNbV-steel and 612–631 °C in the CrNbV-steel. These values can decrease by 40–70 °C, if 0.06 wt. % of Nb additions and 30 °C·s^{-1} cooling rate are taken into account [58,59], reaching ~560 °C in the MoNbV-steel and ~565 °C in the CrNbV-steel. A possible effect of deformation on B_s is difficult to assess quantitatively. Although it is known that pre-strain may increase B_s [60], due to an increase in the number of bainite nucleation sites, and retard the bainite transformation rate following mechanical stabilisation of austenite [61,62]. Thus, it is obvious that for 500 °C finish cooling/holding temperature we observed the bainitic microstructure in both steels. However, the Mo and Cr additions, and strain variation did show some effects on: (i) dislocation structure in the bainitic ferrite and morphology of martensite; and (ii) particle precipitation. Consequently, the mechanical properties varied.

4.1. Strain Effect on Phase Transformation and Precipitation

In both steels, higher strains should have enhanced DRX (dynamic recrystallization) and strain induced precipitation. Although, the absolute values of grain size, particle number density and solid solute concentrations could have been expected to differ with Mo and Cr contents. Thus, with strain increase: (i) the average dislocation density in bainitic ferrite decreased in both steels; (ii) dislocation cell arrangements did not form in the MoNbV-steel and disintegrated walls were present instead; (iii) the fraction of martensite decreased in both steels, although by a different value: by 1.8 times in the MoNbV-steel and by 15% in the CrNbV-steel; and (iv) the average and maximum sizes of blocky and elongated crystals of martensite either remained constant or decreased in the MoNbV-steel, although they have increased in the CrNbV-steel. All these could be explained if after higher strain processing and more intense dynamic recrystallization of austenite (DRX) the prior austenite grain size (PAGS) was smaller in the MoNbV-steel, due to more effective grain boundary pinning by Mo solute atoms, and coarser in the CrNbV-steel, due to grain growth. Smaller PAGS would increase B_s temperature and help nucleation of the bainitic ferrite. With sufficient holding time, this would result in a low retained austenite fraction available for the martensitic transformation. A slightly lower dislocation density in bainitic ferrite after high strain schedule compared to the low strain one (Table 1), could be explained by the increased B_s temperature and longer time at high temperature available for re-arrangement of dislocations after bainitic ferrite formation.

With strain increase the >20 nm particles area fraction and number density increased and the <20 nm volume fraction and number density decreased in both steels. This indicates faster nucleation and growth of precipitates for the higher strain schedule. In addition, the amount of Mo-containing particles in the MoNbV-steel increased with strain. All these support the expected intensification of strain induced precipitation of NbV-containing particles in both steels and Mo-containing ones in the MoNbV-steel with strain increase.

Enhancement of strain induced precipitation should have resulted in decreased element concentrations in solid solution and possible prior austenite strength decrease. If this occurred, low strength austenite would be faster transforming to bainite (faster growth of the bainitic ferrite would take place) [54], resulting in a lower fraction of retained austenite available for the transformation to martensite during cooling to room temperature after holding. This could be another reason, in addition to PAGS size variation, leading to a decreased fraction of martensite after the higher strain processing.

4.2. Mo and Cr Effects on Phase Transformation

For the low strain schedule, we observed insignificant effect of 0.2 wt. % Mo or Cr additions on phase characteristics, in particular, the average size of bainitic ferrite areas, dislocation density in bainitic ferrite, size of blocky and elongated grains of martensite, and martensite fraction. Although, the maximum sizes of blocky and elongated martensite slightly increased with Mo content. This could result from the variation in recrystallization stop temperature, T_{nr}, and prior austenite grain size (PAGS) in the studied steels. Our measurements have shown T_{nr} to be higher in the MoNbV-steel, ~1000 °C, compared to the CrNbV-steel, ~975 °C, which is in-line with Mo being a stronger recrystallization retarding element than Cr [36,37]. Therefore, after 0.3 strain at 1175 °C and 0.35 strain at 1100 °C (modest strain levels with respect to the rate of DRX) the PAGS could be slightly larger in the MoNbV-steel as a result of partial DRX. A larger PAGS would result in a larger size of austenite retained after holding at 500 °C and, subsequently, a coarser martensite formed during the final cooling to the room temperature. Presence of diverse dislocation structure (cell walls) in the MoNbV-steel after low strain processing could also result from a larger PAGS. Larger PAGS was observed accelerating the bainite growth rate in low carbon steels [63].

For the high strain schedule, the effect of steel composition on microstructure was more pronounced. Mo addition led to a decreased size (average and maximum) and lower fraction of martensite. This could be explained if after a higher strain PAGS was smaller in the MoNbV-steel (opposite trend to the low strain schedule). High strain levels would increase the rate of DRX in both steels. However, in the MoNbV-steel the recrystallized fine grain size would be preserved by Mo solute atoms pinning the grain boundaries and preventing the grain growth. In contrast, the solute drag effect of Cr atoms was weaker and the grain growth took place in the CrNbV-steel. Smaller PAGS (larger grain boundary area) can facilitate nucleation of bainitic ferrite and increase the Bs temperature [64]. Therefore, in the MoNbV-steel smaller PAGS resulted in smaller size and lower fraction of the martensite.

4.3. Mo and Cr Effects on Precipitation

The effect of 0.2 wt. % Mo addition on precipitation was more pronounced than that of 0.2 wt. % Cr. In the MoNbV-steel, Mo was present in >20 nm particles, although in the CrNbV-steel Cr did not precipitate. The number density and area fraction of >20 nm Mo/MoNbV-containing particles were 3.5 and 2 times lower, for the low strain schedule, and 1.8 and 3.7 times lower, for the high strain schedule, in the MoNbV-steel compared to the corresponding parameters of Nb/NbV-containing particles in the CrNbV-steel. This indicates a stronger potential of Mo to increase solubility of C and possibly of Nb and V in austenite than that of Cr, thus delaying the precipitation. The effect of Mo addition on the C solubility was reported previously [65].

The number density and volume fraction of <20 nm Fe_3C particles were 1.6 and 3 times lower, for the low strain schedule, and 1.7 and 1.5 times lower, for the high strain schedule, in the MoNbV-steel. This suggests a stronger ability of Mo to retard Fe_3C precipitation than this of Cr. A combination of several factors might be responsible for this. The tendency for C atoms to form Mo-C dipoles in preference to Fe-C ones was reported previously [66]. This is linked to a higher binding energy between Mo-C atoms (0.45–0.5 eV [67]) compared to the binding energy between the Fe and C in cementite (0.40–0.42 eV [68,69]). A higher binding energy means that a higher activation energy is required for C atom to jump into another position. The carbon diffusivity in Fe also changes in the presence of different solutes and it was reported for both Cr and Mo that the activation enthalpy for carbon diffusion in iron increases [70–72]. However, the carbon diffusivity in ferrite was decreased more in the presence of Mo than of Cr [73]. Absence of Mo-, Cr-, Nb- or V-rich particle precipitation in the <20 nm size range in both steels increased concentrations of these elements, carbon and, maybe, nitrogen in solid solution. In addition, the solid solute concentrations could be higher in the MoNbV-steel, due to less developed precipitation. This would correspond to a larger unit cell expansion of the bainitic ferrite in the MoNbV-steel (0.310–0.312 nm) than that in the CrNbV-steel (0.306–0.308 nm). A larger

effect of Mo than Cr on Fe lattice expansion is related to larger atom radius mismatch between Fe (126 pm) and Mo (139 pm) than between Fe and Cr (128 pm) [74].

4.4. Microstructure-Mechanical Properties Relationship: Role of Solute Atoms

In spite of similar phase balance, grain size and dislocation density, and less pronounced precipitation, the MoNbV-steel exhibited higher strength than the CrNbV-steel for both processing conditions (Table 1). This could result from higher solid solution strengthening from Mo, Cr, Nb, V, C and N atoms in the MoNbV-steel. To clarify this the contributions to yield stress from various microstructural parameters have been calculated as follows:

- from grain boundaries using the Hall–Petch equation:

$$\sigma_{gs} = \sigma_0 + k \cdot d^{-1/2},$$

where σ_0 = 15 MPa and k = 21.4 MPa·mm$^{1/2}$ are accepted for pure iron [75], and d is the size of bainitic ferrite areas (the shortest distance between the martensitic grains);
- from precipitation of >20 nm particles using the Ashby-Orowan equation [76], which assumes the dislocation looping around relatively large particles:

$$\Delta\sigma_{ps1} = \frac{10.8\sqrt{f}}{D} \ln\left(\frac{D}{6.125 \times 10^{-4}}\right),$$

where f is the particle volume fraction and D is the particle diameter in μm;
- from precipitation of <20 nm particles using the order strengthening relationship [77], which assumes the dislocation cutting of relatively small, coherent particles:

$$\Delta\sigma_{ps2} = 0.81 \cdot M \cdot \frac{\gamma}{2b} \cdot \left(\frac{3\pi f}{8}\right)^{0.5},$$

where M = 3 is the matrix orientation factor, b = 0.312–0.306 nm is Burgers vector accepted according to the measured unite cell size of bainitic ferrite (Table 1), γ is the matrix-particle interface energy assumed for the Fe-Fe_3C interface to be γ = 0.5 J·m^{-2} [78], and f is the particle volume fraction;
- from dislocations using the long range work hardening theory [79]:

$$\Delta\sigma_{wh} = \frac{\alpha}{2\pi} G b \sqrt{\rho},$$

where α = 0.5 is a constant, G = 85,000 MPa is the shear modulus, b = 0.312–0.306 nm is the Burgers vector and ρ is the measured dislocation density;
- the solid solution strengthening contribution from Mn and Si was estimated using the matrix concentrations of these elements and the following relationship [76]:

$$\Delta\sigma_{ss(Si,Mn)} = 83C_{Si} + 32C_{Mn},$$

where C_{Si} = 0.3 wt. % and C_{Mn} = 1.5 wt. % are Si and Mn concentrations in the bainitic ferrite matrix, respectively.

A possible effect of martensite on the yield stress of studied steels was neglected in the calculation, due to the martensite requiring higher stresses and strains, than bainitic ferrite, to start yielding.

As can be seen from Table 2, for both steels the major contribution to the YS was coming from grain boundary strengthening, which is quite reasonable for the size of bainitic ferrite areas being below 1 μm. Contributions from dislocations were in the same range of values, which is in-line with similar dislocation densities measured in the studied steels. The solid solution strengthening from Si

and Mn was the same for all four conditions, because the contents of these elements were similar in both steels and their precipitation was not observed. For three cases, namely the CrNbV-steel in both processing conditions and the MoNbV-steel after high strain processing, calculations overestimated the yield stress (a negative value for the difference between the measured and total calculated yield stress, Δ, was observed, Table 2). This can be related to two major reasons: (i) incomplete number of dislocation-obstacle interactions really occurring, compared to the theoretical maximum assumed in the applied equations; and (ii) the material inhomogeneity. Some volumes of the bainitic ferrite matrix could be softer, due to lower solute atom concentrations or/and lower number density of precipitates or/and lower dislocation density. These softer volumes would start yielding first. However, for the MoNbV-steel processed according to the lower strain schedule the measured yield stress was 89 MPa (~12%) higher than the calculated value. This is in contrast to the lowest precipitation strengthening contribution calculated for the MoNbV-steel subjected to the lower strain processing. The additional strengthening in this condition could originate from two sources: (i) solid solute atoms of Mo, C and, possibly, N; and (ii) atom clusters of Mo, Nb and V. Substantial strengthening from atom clusters was recently reported for microalloyed steels [80–83]. In spite of qualitatively similar effects of Mo and Cr on solubility of other elements, in the CrNbV-steel a possible strengthening from solute atoms and atom clusters did not exhibit itself. Obviously, a quantitatively weaker effect of Cr on solubility resulted in more pronounced precipitation and lower concentrations of microalloying elements available for solid solution and cluster strengthening.

Table 2. Calculated contributions to the yield stress in the studied steels.

Steel	Strain	Calculated Contributions						Experimental YS	Δ *
		Grain Boundaries #	Particles		Dislocation Density	Solid Solute (Si, Mn)	Total		
			>20 nm	>20 nm					
MoNbV	Low	586	19	21	62	73	761	850	+89
	High	618	31	30	42	73	794	775	−19
CrNbV	Low	675	37	37	58	73	880	765	−115
	High	595	52	37	40	73	797	700	−97

For the largest areas of bainitic ferrite; * Δ is the difference between the experimental and total calculated yield stress values.

For both steels, the measured yield stress decreased with an increase in strain during processing. In the CrNbV-steel this corresponds to the decrease in grain size strengthening contribution (in trend and value). However, in the MoNbV-steel the grain size and precipitation strengthening contributions increased with strain. Obviously, in the MoNbV-steel these contributions did not compensate for the decreased solid solution/cluster strengthening. This indicates a significant role of solid solute atoms and atom clusters as strengthening agents in bainitic microalloyed steels. With an increase in dislocation density, associated with bainitic microstructure, a potential number of dislocation-atom/cluster interaction sites may increase faster than the number of dislocation-precipitate interaction sites, due to a very high density of atoms/clusters. Thus, the role of solute concentrations increases in bainitic microstructures compared to the ferritic.

In the CrNbV-steel coarser martensite could be expected to decrease elongation for the higher strain processing. However, an opposite trend was observed: the elongation has increased in the CrNbV-steel for the higher strain schedule. This could have been related to more intensive dislocation generation in the CrNbV-steel during tensile testing, leading to more homogeneous slip and delated local micro-crack formation. The dislocation generation in the CrNbV-steel would be associated with the increased number density of >20 nm particles for this processing condition. Nano-precipitates were reported to stimulate dislocation generation [84,85].

Based on these a final conclusion can be made with respect to the design of steel composition: if a bainitic steel is required to exhibit superior strength, Mo should be used as a microalloying element,

because it increases the solubility of other microalloying elements and increases the solid solution and cluster strengthening effects; if a bainitic steels is required to exhibit higher ductility, Cr can be used to facilitate bainite transformation but allow precipitation to take place.

5. Conclusions

Comparative study of Mo and Cr effects on microstructure and mechanical properties of newly developed NbV-microalloyed bainitic steels has shown the following:

1. Additions of either 0.2 wt. % Mo or 0.2 wt. % Cr (above 0.3 wt. % Cr) resulted in formation of bainite microstructure with mixed bainite morphologies and similar parameters of bainitic ferrite matrix and martensite as the second phase. However, for higher strain processing (when the DRX may be completed faster) the size and fraction of martensite were lower in the MoNbV-steel. This could be related to a smaller prior austenite grain size in the MoNbV-steel, which would correspond to a stronger solute drag effect of Mo during DRX. The influence of prior austenite grain size on bainite phase transformation in the studied steels requires further investigation.
2. The number density and area fraction of >20 nm NbV-containing particles were significantly lower in the MoNbV-steel. This supports a stronger effect of Mo than Cr on the increase of solubility of Nb and V in austenite, which results in their decreased precipitation. The number density and area fraction of <20 nm Fe_3C particles were also lower in the MoNbV-steel. This supports a stronger effect of Mo than Cr on the retardation of Fe_3C precipitation. Less pronounced precipitation in the MoNbV-steel, and related to this increased solid solute concentrations, corresponds to a wider expansion of the unit cell size of the bcc lattice of bainitic ferrite matrix.
3. In addition to grain size strengthening, the solid solution/atom cluster strengthening effect was the second dominating in the MoNbV-steel; although in the CrNbV-steel the precipitation strengthening from >20 nm particles, <20 nm particles and dislocations equally contributed to the overall steel strength.
4. Strain increase resulted in more pronounced strain induced precipitation of Mo, Nb and V in the MoNbV-steel and Nb and V in the CrNbV-steel. Solute depletion in microalloying elements could have contributed to decreased strength levels in both steels for the higher strain processing schedule.

Acknowledgments: This project was financially supported by the ARC Research Hub for Australian Steel Manufacturing and, in particular, by Bluescope Steel Ltd. (Melbourne, Australia). The microscopy was carried out using JEOL JSM-7001F FEGSEM (supported by grant No. LE0882613) and JEOL JEM-2011 TEM (supported by grant No. LE0237478) microscopes at the Electron Microscopy Centre at the University of Wollongong.

Author Contributions: Andrii Kostryzhev has conceived the idea, conducted the microstructure characterisation and analysis of the microstructure-properties relationship, and has written the paper. Navjeet Singh and Liang Chen carried out the sample processing in Gleeble. Navjeet Singh conducted the tensile testing. Chris Killmore and Elena Pereloma carried out the overall project management, participated in discussion of the results, and contributed to the paper writing.

Conflicts of Interest: The authors declare no conflict of interest.

References

1. Aaronson, H.I.; Reynolds, W.T., Jr.; Purdy, G.R. The incomplete transformation phenomenon in steel. *Metall. Mater. Trans. A* **2006**, *37*, 1731–1745. [CrossRef]
2. Humphreys, E.S.; Fletcher, H.A.; Hutchins, J.D.; Garratt-Reed, A.J.; Reynolds, W.T., Jr.; Aaronson, H.I.; Purdy, G.R.; Smith, G.D.W. Molybdenum accumulation at ferrite: Austenite interfaces during isothermal transformation of an Fe-0.24 pct C-0.93 pct Mo alloy. *Metall. Mater. Trans. A* **2004**, *35*, 1223–1235. [CrossRef]
3. Kong, J.; Xie, C. Effect of molybdenum on continuous cooling bainite transformation of low-carbon microalloyed steel. *Mater. Des.* **2006**, *27*, 1169–1173. [CrossRef]
4. Hu, H.; Xu, G.; Zhou, M.; Yuan, Q. Effect of Mo content on microstructure and property of low-carbon bainitic steels. *Metals* **2016**, *6*, 173. [CrossRef]

5. Sung, H.-K.; Lee, D.-H.; Shin, S.-Y.; Lee, S.; Yoo, J.-Y.; Hwang, B. Effect of finish cooling temperature on microstructure and mechanical properties of high-strength bainitic steels containing Cr, Mo and B. *Mater. Sci. Eng. A* **2015**, *624*, 14–22. [CrossRef]
6. Uemori, R.; Chijiiwa, R.; Tamehiro, H.; Morikawa, H. AP-FIM study on the effect of Mo addition on microstructure in Ti-Nb steel. *Appl. Surf. Sci.* **1994**, *76*, 255–260. [CrossRef]
7. Wan, R.; Sun, F.; Zhang, L.; Shan, A. Effect of Mo addition on strength of fire-resistant steel at elevated temperature. *J. Mater. Eng. Perform.* **2014**, *23*, 2780–2786. [CrossRef]
8. Dimitriu, R.C.; Bhadeshia, H.K.D.H. Hot strength of creep resistant ferritic steels and relationship to creep rupture data. *Mater. Sci. Technol.* **2007**, *23*, 1127–1131. [CrossRef]
9. He, R.; Jiang, L.; Dong, W. Development of high corrosion-resistant ferritic stainless steel and its application in the building cladding system. *Baosteel Tech. Res.* **2013**, *7*, 54–58.
10. Akben, M.G.; Bacroix, B.; Jonas, J.J. Effect of vanadium and molybdenum addition on high temperature recovery, recrystallization and precipitation behaviour of niobium-based microalloyed steels. *Acta Metall.* **1983**, *31*, 161–174. [CrossRef]
11. Andrade, H.L.; Akben, M.G.; Jonas, J.J. Effect of molybdenum, niobium, and vanadium on static recovery and recrystallization and on solute strengthening in microalloyed steels. *Metall. Trans. A* **1983**, *14*, 1967–1977. [CrossRef]
12. Schambron, T.; Chen, L.; Gooch, T.; Dehghan-Manshadi, A.; Pereloma, E.V. Effect of Mo concentration on dynamic recrystallization behavior of low carbon microalloyed steels. *Steel Res. Int.* **2013**, *84*, 1191–1195. [CrossRef]
13. Lu, J.; Omotoso, O.; Wiskel, J.B.; Ivey, D.G.; Henein, H. Strengthening mechanisms and their relative contributions to the yield strength of microalloyed steels. *Metall. Mater. Trans. A* **2012**, *43*, 3043–3061. [CrossRef]
14. Zhou, X.; Liu, C.; Yu, L.; Liu, Y.; Li, H. Phase transformation behavior and microstructural control of high-Cr martensitic/ferritic heat-resistant steels for power and nuclear plants: A review. *J. Mater. Sci. Technol.* **2015**, *31*, 235–242. [CrossRef]
15. Wang, Q.; Zhang, C.; Li, R.; Gao, J.; Wang, M.; Zhang, F. Characterization of the microstructures and mechanical properties of 25CrMo48V martensitic steel tempered at different times. *Mater. Sci. Eng. A* **2013**, *559*, 130–134. [CrossRef]
16. Chen, C.Y.; Chen, C.C.; Yang, J.R. Microstructure characterization of nanometer carbides heterogeneous precipitation in Ti–Nb and Ti–Nb–Mo steel. *Mater. Charact.* **2014**, *88*, 69–79. [CrossRef]
17. Mukherjee, S.; Timokhina, I.; Zhu, C.; Ringer, S.P.; Hodgson, P.D. Clustering and precipitation processes in a ferritic titanium-molybdenum microalloyed steel. *J. Alloy. Compd.* **2017**, *690*, 621–632. [CrossRef]
18. Wang, Z.; Zhang, H.; Guo, C.; Liu, W.; Yang, Z.; Sun, X.; Zhang, Z.; Jiang, F. Effect of molybdenum addition on the precipitation of carbides in the austenite matrix of titanium micro-alloyed steels. *J. Mater. Sci.* **2016**, *51*, 4996–5007. [CrossRef]
19. Larzabal, G.; Isasti, N.; Rodriguez-Ibabe, J.M.; Uranga, P. Evaluating strengthening and impact toughness mechanisms for ferritic and bainitic microstructures in Nb, Nb-Mo and Ti-Mo microalloyed steels. *Metals* **2017**, *7*, 65. [CrossRef]
20. Lee, W.-B.; Hong, S.-G.; Park, C.-G.; Park, S.-H. Carbide precipitation and high-temperature strength of hot-rolled high-strength, low-alloy steels containing Nb and Mo. *Metall. Mater. Trans. A* **2002**, *33*, 1689–1698. [CrossRef]
21. Jang, J.H.; Heo, Y.-U.; Lee, C.-H.; Bhadeshia, H.K.D.H.; Suh, D.-W. Interphase precipitation in Ti–Nb and Ti–Nb–Mo bearing steel. *Mater. Sci. Technol.* **2013**, *29*, 309–313. [CrossRef]
22. Funakawa, Y.; Shiozaki, T.; Tomita, K.; Yamamoto, T.; Maeda, E. Development of high strength hot-rolled sheet steel consisting of ferrite and nanometer-sized carbides. *ISIJ Int.* **2004**, *44*, 1945–1951. [CrossRef]
23. Park, D.-B.; Huh, M.-Y.; Shim, J.-H.; Suh, J.-Y.; Lee, K.-H.; Jung, W.-S. Strengthening mechanism of hot rolled Ti and Nb microalloyed HSLA steels containing Mo and W with various coiling temperature. *Mater. Sci. Eng. A* **2013**, *560*, 528–534. [CrossRef]
24. Bracke, L.; Xu, W. Effect of the Cr content and coiling temperature on the properties of hot rolled high strength lower bainitic steel. *ISIJ Int.* **2015**, *55*, 2206–2211. [CrossRef]
25. Lee, H.-J.; Lee, H.-W. Effect of Cr content on microstructure and mechanical properties of low carbon steel welds. *Int. J. Electrochem. Sci.* **2015**, *10*, 8028–8040.

26. Zhou, M.; Xu, G.; Tian, J.; Hu, H.; Yuan, Q. Bainitic transformation and properties of low carbon carbide-free bainitic steels with Cr addition. *Metals* **2017**, *7*, 263. [CrossRef]
27. Mishra, S.K.; Das, S.; Ranganathan, S. Precipitation in high strength low alloy (HSLA) steel: A TEM study. *Mater. Sci. Eng. A* **2002**, *323*, 285–292.
28. Janovec, J.; Svoboda, M.; Vyrostkova, A.; Kroupa, A. Time-temperature-precipitation diagrams of carbide evolution in low alloy steels. *Mater. Sci. Eng. A* **2005**, *402*, 288–293. [CrossRef]
29. Timokhina, I.B.; Hodgson, P.D.; Ringer, S.P.; Zheng, R.K.; Pereloma, E.V. Precipitate characterisation of an advanced high-strength low-alloy (HSLA) steel using atom probe tomography. *Scr. Mater.* **2007**, *56*, 601–604. [CrossRef]
30. Gorokhova, N.A.; Sarrak, V.I.; Suvorova, S.O. Solubility of titanium and niobium carbides in high-chromium ferrite. *Met. Sci. Heat Treat.* **1986**, *28*, 276–279. [CrossRef]
31. Tsai, S.-P.; Su, T.-C.; Yang, J.-R.; Chen, C.-Y.; Wang, Y.-T.; Huang, C.-Y. Effect of Cr and Al additions on the development of interphase-precipitated carbides strengthened dual-phase Ti-bearing steels. *Mater. Des.* **2017**, *119*, 319–325. [CrossRef]
32. Koyama, S.; Ishii, T.; Narita, K. Effects of Mn, Si, Cr and Ni on the solution and precipitation of Niobium carbide in iron austenite. *J. Jpn. Inst. Met.* **1971**, *35*, 1089–1094. [CrossRef]
33. Ray, A. Niobium microalloying in rail steel. *Mater. Sci. Technol.* **2017**, *33*, 1584–1600. [CrossRef]
34. Pereloma, E.V.; Bata, V.; Scott, R.I.; Smith, R.M. Effect of Cr on strain ageing behaviour of low carbon steel. *Mater. Sci. Forum* **2007**, *539–543*, 4214–4219. [CrossRef]
35. Lu, Q.; Xu, W.; van der Zwaag, S. Designing new corrosion resistant ferritic heat resistant steel based on optimal solid solution strengthening and minimisation of undesirable microstructural components. *Comput. Mater. Sci.* **2014**, *84*, 198–205. [CrossRef]
36. Yamamoto, S.; Sakiyama, T.; Ouchi, C. Effect of alloying elements on recrystallization kinetics after hot deformation in austenitic stainless steels. *Trans. ISIJ* **1987**, *27*, 447–452. [CrossRef]
37. De Abreu Martins, C.; Poliak, E.; Godefroid, L.B.; Fonstein, N. Determining the conditions for dynamic recrystallization in hot deformation of C–Mn–V steels and the effects of Cr and Mo additions. *ISIJ Int.* **2014**, *54*, 227–234. [CrossRef]
38. Hutchinson, B.; Siwecki, T.; Komenda, J.; Hagström, J.; Lagneborg, R.; Hedin, J.-E.; Gladh, M. New vanadium-microalloyed bainitic 700 MPa strip steel product. *Ironmak. Steelmak.* **2014**, *41*, 1–6. [CrossRef]
39. Kong, X.; Lan, L.; Hu, Z.; Li, B.; Sui, T. Optimization of mechanical properties of high strength bainitic steel using thermo-mechanical control and accelerated cooling process. *J. Mater. Process. Technol.* **2015**, *217*, 202–210. [CrossRef]
40. Abbasi, E.; Rainforth, W.M. Effect of Nb-Mo additions on precipitation behaviour in V microalloyed TRIP-assisted steels. *Mater. Sci. Technol.* **2016**, *32*, 1721–1729. [CrossRef]
41. Sourmail, T. Precipitation in creep resistant austenitic stainless steels. *Mater. Sci. Technol.* **2001**, *17*, 1–14. [CrossRef]
42. Williams, D.; Carter, C.B. *Transmission Electron Microscopy II—Diffraction*; Plenum Press: New York, NY, USA, 1996; pp. 321–323.
43. Pereloma, E.V.; Al-Harbi, F.; Gazder, A. The crystallography of carbide-free bainites in thermo-mechanically processed low Si transformation-induced plasticity steels. *J. Alloy. Compd.* **2014**, *615*, 96–110. [CrossRef]
44. Pandit, A.; Murugaiyan, A.; Saha Podder, A.; Haldar, A.; Bhattacharjee, D.; Chandra, S.; Ray, R.K. Strain induced precipitation of complex carbonitrides in Nb–V and Ti–V microalloyed steels. *Scr. Mater.* **2005**, *53*, 1309–1314. [CrossRef]
45. Cabibbo, M.; Fabrizi, A.; Merlin, M.; Garagnani, G.L. Effect of thermo-mechanical treatments on the microstructure of micro-alloyed low-carbon steels. *J. Mater. Sci.* **2008**, *43*, 6857–6865. [CrossRef]
46. Kostryzhev, A.G.; Strangwood, M.; Davis, C.L. Mechanical property development during UOE forming of large diameter pipeline steels. *Mater. Manuf. Process.* **2010**, *25*, 41–47. [CrossRef]
47. Miyata, K.; Omura, T.; Kushida, T.; Komizo, Y. Coarsening kinetics of multicomponent MC-type carbides in high-strength low-alloy steels. *Metall. Mater. Trans. A* **2003**, *34*, 1565–1573. [CrossRef]
48. Jack, D.H.; Jack, K.H. Carbides and nitrides in steel. *Mater. Sci. Eng.* **1973**, *11*, 1–27. [CrossRef]
49. Bagaryatskii, Y.A. Probable mechanism of martensite decomposition. *Dokl. Acad. Nauk SSSR* **1950**, *73*, 1161–1164. (In Russian)
50. Andrews, K.W. Tabulation of interplanar spacings of cementite Fe_3C. *Acta Crystallogr.* **1963**, *16*, 68. [CrossRef]

51. Agrawal, B.K. *Introduction to Engineering Materials*; Tata McGraw-Hill: New Delhi, India, 1988.
52. Irvine, J.; Baker, T.N. The influence of rolling variables on the strengthening mechanisms operating in Niobium steels. *Mater. Sci. Eng.* **1984**, *64*, 123–134. [CrossRef]
53. Khalid, E.A.; Edmonds, D.V. Mixed structures in continuously cooled low-carbon automotive steels. *J. Phys. IV* **1993**, *3*, 147–152. [CrossRef]
54. Garcia-Mateo, C.; Caballero, F.G.; Capdevila, C.; Garcia de Andres, C. Estimation of dislocation density in bainitic microstructures using high-resolution dilatometry. *Scr. Mater.* **2009**, *61*, 855–858.
55. Stevens, W.; Haynes, A.G. The temperature of formation of martensite and bainite in low-alloy steel. *J. Iron Steel Inst.* **1956**, *183*, 349–359.
56. Kunitake, T.; Okada, Y. The estimation of bainite transformation temperatures in steels by the empirical formulas. *J. Iron Steel Inst. Jpn.* **1998**, *84*, 137–141. [CrossRef]
57. Lee, Y.-K. Empirical formula of isothermal bainite start temperature of steel. *J. Mater. Sci. Lett.* **2002**, *21*, 1253–1255. [CrossRef]
58. Lee, Y.-K.; Hong, J.-M.; Choi, C.-S.; Lee, J.-K. Continuous cooling transformation temperatures and microstructures of niobium bearing microalloyed steels. *Mater. Sci. Forum* **2005**, *475–479*, 65–68.
59. Carpenter, K.R.; Killmore, C.R. The effect of Nb on the continuous cooling transformation curves of ultra-thin strip CASTRIP© Steels. *Metals* **2015**, *5*, 1857–1877. [CrossRef]
60. Lambers, H.G.; Tschumak, S.; Maier, H.J.; Canading, D. Role of austenization and pre-deformation on the kinetics of the isothermal bainite transformation. *Metall. Mater. Trans. A* **2009**, *40*, 1355–1366. [CrossRef]
61. Larn, R.H.; Yang, J.R. The effect of compressive deformation of austenite on the bainitic ferrite transformation in Fe-Mn-Si-C steels. *Mater. Sci. Eng. A* **2000**, *278*, 278–291. [CrossRef]
62. Bhadeshia, H.K.D.H. *Bainite in Steels*; IOM Communications: London, UK, 2001; p. 221.
63. Matsuzaki, A.; Bhadeshia, H.K.D.H. Effect of austenite grain size and bainite morphology on overall kinetics of bainite transformation in steels. *Mater. Sci. Technol.* **1999**, *15*, 518–522. [CrossRef]
64. Kang, S.; Yoon, S.; Lee, S.-J. Prediction of bainite start temperature in alloy steels with different grain sizes. *ISIJ Int.* **2014**, *54*, 997–999. [CrossRef]
65. Wada, H.; Pehlke, R.D. Nitrogen solubility and nitride formation in austenitic Fe-Ti alloys. *Matall. Trans. B* **1985**, *16*, 815–822. [CrossRef]
66. Tagashira, K.; Mutsuji, T.; Endo, T. Effect of Mo-C dipole on the development of {111} recrystllisation texture in Mo added low carbon steels. *Tetsu-to-Hagané* **2000**, *86*, 466–471. [CrossRef]
67. Bata, V. Minimising Ageing due to Carbon in Low Carbon Sheet Steel with the Aid of Mn, Cr, Mo or B Addition. Ph.D. Thesis, Monash University, Melbourne, Australia, June 2006.
68. Johnson, R.A.; Diens, G.I.; Damask, A.C. Calculations of the energy and migration characteristics of carbon and nitrogen in α-iron and vanadium. *Acta Metall.* **1964**, *12*, 1215–1224. [CrossRef]
69. Johnson, R.A. Clustering of carbon atoms in α-iron. *Acta Metall.* **1967**, *15*, 513–517. [CrossRef]
70. Liu, P.; Xing, W.; Cheng, X.; Li, D.; Li, Y.; Chen, X.-Q. Effects of dilute substitutional solutes on interstitial carbon in α-Fe: Interactions and associated carbon diffusion from first-principles calculations. *Phys. Rev. B* **2014**, *90*, 024103. [CrossRef]
71. Golovin, I.S.; Blanter, M.S.; Magalas, L.B. Interactions of dissolved atoms and carbon diffusion in Fe-Cr and FeAl alloys. *Defect Diffus. Forum* **2001**, *194–199*, 73–78. [CrossRef]
72. Pereloma, E.V.; Bata, V.; Scott, R.I.; Smith, R.M. Effect of Cr and Mo on strain ageing behaviour of low carbon steel. *Mater. Sci. Eng. A* **2010**, *527*, 2538–2546. [CrossRef]
73. Sandomirskij, M.M.; Grigorkin, V.I.; Zemskij, S.V. Alloying element effect on carbon diffusion in ferrite of pearlitic steel at tempering. *Izv. Vysshikh Uchebnykh Zavedenij. Chernaya Metall.* **1985**, *5*, 116–119.
74. Fleischer, R.L. Solution hardening. *Acta Metall.* **1961**, *9*, 996–1000. [CrossRef]
75. Dingly, D.J.; McLean, D. Components of the flow stress of iron. *Acta Metall.* **1967**, *15*, 885–901. [CrossRef]
76. Gladman, T. *The Physical Metallurgy of Microalloyed Steels*; The Institute of Materials, Cambridge University Press: Cambridge, UK, 1997.
77. Seidman, D.N.; Marquis, E.A.; Dunand, D.C. Precipitation strengthening at ambient and elevated temperatures of heat-treatable Al(Sc) alloys. *Acta Mater.* **2002**, *50*, 4021–4035. [CrossRef]
78. Zhang, X.; Hickel, T.; Rogal, J.; Fähler, S.; Drautz, R.; Neugebauer, J. Structural transformations among austenite, ferrite and cementite in Fe–C alloys: A unified theory based on ab initio simulations. *Acta Mater.* **2015**, *99*, 281–289. [CrossRef]

79. Argon, A.S. Mechanical properties of single-phase crystalline media: Deformation at low temperature. In *Physical Metallurgy*; Cahn, R.W., Haasen, P., Eds.; North-Holland Publishing: Amsterdam, The Netherlands, 1996.
80. Timokhina, I.B.; Enomoto, M.; Miller, M.K.; Pereloma, E.V. Microstructure-property relationship in the thermomechanically processed C-Mn-Si-Nb-Al-(Mo) transformation-induced plasticity steels before and after prestraining and bake hardening treatment. *Metall. Mater. Trans. A* **2012**, *43*, 2473–2483. [CrossRef]
81. Xie, K.Y.; Zheng, T.; Cairney, J.M.; Kaul, H.; Williams, J.G.; Barbaro, F.J.; Killmore, C.R.; Ringer, S.P. Strengthening from Nb-rich clusters in a Nb-microalloyed steel. *Scr. Mater.* **2012**, *66*, 710–713. [CrossRef]
82. Kostryzhev, A.G.; Al Shahrani, A.; Zhu, C.; Cairney, J.M.; Ringer, S.P.; Killmore, C.R.; Pereloma, E.V. Effect of niobium clustering and precipitation on strength of a NbTi-microalloyed ferritic steel. *Mater. Sci. Eng. A* **2014**, *607*, 226–235. [CrossRef]
83. Zhang, Y.-J.; Miyamoto, G.; Shinbo, K.; Furuhara, T.; Ohmura, T.; Suzuki, T.; Tsuzaki, K. Effects of transformation temperature on VC interphase precipitation and resultant hardness in low-carbon steels. *Acta Mater.* **2015**, *84*, 375–384. [CrossRef]
84. Hansen, N.; Barlow, C.Y. Microstructure evolution in whisker- and particle-containing materials. In *Fundamentals of Metal-Matrix Composites*; Surech, S., Mortensen, A., Needleman, A., Eds.; Elsevier: Boston, MA, USA, 1993; pp. 109–118.
85. Humphreys, F.J.; Hatherly, M. *Recrystallisation and Related Annealing Phenomena*; Elsevier: Oxford, UK, 2004.

© 2018 by the authors. Licensee MDPI, Basel, Switzerland. This article is an open access article distributed under the terms and conditions of the Creative Commons Attribution (CC BY) license (http://creativecommons.org/licenses/by/4.0/).